RSC Advances

PAPER

Solar-Driven Broad Spectrum Fungicides Based on Monodispersed Cu_7S_4 Nanorods with Strong Near-Infrared Photothermal Efficiency

Cite this:

Gaofei Hu,*[a] Tiantian Xu,[a] Xiaoqing Chen,[a] Tony D. James[b] and Suying Xu*[a]

The development of low-cost and biocompatible inorganic photothermal nanoagents with broadband sunlight absorption and high photothermal conversion efficiency as broad spectrum fungicides is highly desirable for the large scale antibacterial treatment especially in the wild, because of their highly efficient anti-bacteria ability *via* solar irradiation. Here, we present a facile strategy for the synthesis of Cu_7S_4 nanorods (NRs) with broadband light absorption (300-3300 nm) and high photothermal conversion efficiency (57.8%, 808 nm), and the use of these NRs as broad spectrum fungicides for efficient disinfection using natural sunlight as light source. In the presence of Cu_7S_4 NRs, with natural sunlight irradiation (70 mW/cm^2), both Gram-positive (*S. aureus*) and Gram-negative (*E. coli*) bacterium strains (2 mL, 10^6 CFU/mL) were completely killed in 10 min. These results suggest that our Cu_7S_4 NRs are effective and broad spectrum photothermal anti-bacterial agents regardless of drug resistance, that are particularly suitable for anti-bacteria activity in the wild using solar irradiation where artificial light sources are not available. Due to their strong near infrared (NIR) absorption, these biocompatible and low-cost Cu_7S_4 NRs may also serve as promising agents for photothermal therapy of tumors, disinfection in clinics, food sterilization and environmental treatment.

Received 00th June 20xx,
Accepted 00th June 20xx
DOI: 10.1039/x0xx00000x
www.rsc.org/

Introduction

The global prevalence of multidrug resistant bacteria (MDRB) is on the rise and makes conventional antibiotic therapies less efficient, which results in great challenges for the biomedical and food technology areas.[1-4] Therefore, it is important to develop easy and highly efficient broad spectrum antibacterial treatments and therapies to fight new bacterial infections regardless of drug resistance. Over the past decade, nanomaterials,[5, 6] including silver nanocrystals,[7-9] gold nanoparticles (NPs),[10, 11] metal oxides[12, 13] and graphene,[9, 14, 15] have been used for disinfection. In contrast to the anti-bacteria mechanism of Ag nanomaterials,[16] the disinfection with other nanomaterials is achieved *via* photothermal therapy (PTT) by means of their good photothermal conversion efficiency. PTT[17-23] has been widely used for tumor therapy by converting near infrared (NIR) light from pulsed lasers into heat by virtue of the efficient photothermal conversion of strongly light-absorbing materials such as polyaniline,[24, 25] gold nanocages,[26-28] gold NRs,[29, 30] gold nanoshells,[31] carbon nanotubes (CNTs),[32] graphene,[33-37] and semiconductors including $Cu_{2-x}S$,[38] $Cu_{2-x}Se$,[39] MoS_2,[40] and WS_2.[41] Moreover, they also were investigated for using solar energy for environmental purification and other fields.[42-46] In order to get the ideal photothermal conversion efficiency, significant effort has been devoted to the controlled synthesis of nanostructures whose absorption peak is in accordance with the laser wavelength, in order to get strong localized surface plasmon resonance (LSPR) absorption.[47-54]

However, due to the inconvenient access to an expensive laser instrument, the application of these agents for *in situ* photothermal treatments was limited in practical situation. Moreover, single-wavelength laser-based photothermal treatments do not satisfy the wide demand for anti-bacterial treatment in the field of large scale food sterilization and environmental treatments. The use of sunlight, as an important source of clean and renewable energy that is abundant in the wild, would be an excellent alternative irradiation for photothermal treatments. However, according to the energy distribution of sunlight, around 54.3%, 38.9% and 6.8% of sunlight at the earth's surface is located in the infrared (760-3000 nm), visible (400-760 nm), and ultraviolet (<400 nm) range, respectively.[55] Therefore, it is highly desirable to develop photothermal agents with broadband, especially strong NIR absorption and high photothermal conversion efficiency, so that these agents can be used for photothermal disinfection by means of natural sunlight. Among the reported photothermal agents, noble metal nanostructures are the most widely investigated materials to date. As a newly emerging type of

[a]*State Key Laboratory of Chemical Resource Engineering, Beijing University of Chemical Technology, Beijing 100029, P. R. China.*
[b]*Depatrment of Chemistry, University of Bath, Bath BA2 7AY, United Kingdom.*
E-mail: hugf@mail.buct.edu.cn; syxu@mail.buct.edu.cn Phone: +86-10-64433197.
Electronic Supplementary Information (ESI) available: Cytotoxicity assessment with and without simulated sunlight irradiation; TEM images of the bacteria; viable counting of the bacteria; photothermal anti-bacteria evaluation under simulated sunlight irradiation for various time intervals. See DOI: 10.1039/x0xx00000x

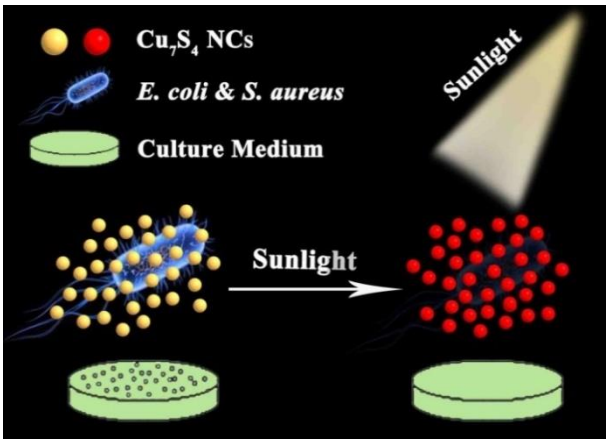

Scheme 1. Schematic diagram of the photothermal anti-bacteria with Cu_7S_4 NCs as broadband absorption and efficient photothermal agents *via* sunlight irradiation.

plasmonic nanomaterial, highly doped *p*-type copper chalcogenides demonstrate excellent photothermal properties because of their strong LSPR effects and broadband absorption.[56] As for a noble metal nanomaterial, with defined nanostructure parameters including metal species, shape, and size, the LSPR response is permanently fixed. Yet, the LSPR peak of the copper chalcogenides can be tuned simply by adjusting the doping levels of carriers.[57] These semiconductor nanocrystals with broad and strong NIR absorption are earth-abundant, low-toxic, photochemical stable, and easy to obtain, therefore would be good alternatives to current photothermal agents.

Herein, we present a facile strategy for the one-step synthesis of hydrophobic Cu_7S_4 nanorods (NRs) *via* hot injection and thermolysis of a single precursor. Compared to our previously prepared Cu_7S_4 nanoparticles (NPs),[56] these Cu_7S_4 NRs with LSPR absorption peak around 1500 nm demonstrate stronger light absorption in the range of 300-3300 nm and higher photothermal conversion efficiency, which is particularly suitable for the photothermal conversion of sunlight. By coating with a lab-made amphiphilic polymer (PSI_{OAm}, oleylamine functionalized polysuccinimide), the hydrophobic Cu_7S_4 NRs were successfully transferred into water as Cu_7S_4@PSI_{OAm} nanocomposites (Cu_7S_4 NCs) for photothermal ablation application. As shown in Scheme 1, the Cu_7S_4 NCs were mixed with bacteria, owning to their good biocompatibility, the viability of bacteria was not influenced in the absence of sunlight irradiation. However, after irradiation with sunlight, the media temperature was dramatically elevated, and thus the Gram-negative (*E. coli*) and Gram-positive (*S. aureus*) pathogens were totally killed, which clearly indicates that these Cu_7S_4 NCs are promising candidates for biocompatible, stable and effective solar photothermal agents used in the disinfection of bacteria.

Experimental section

Chemicals and Reagents.

Oleic acid (OA), oleylamine (OAm) and 1-octadecene (ODE) were purchased from Alfa. Sodium hydroxide (NaOH), ethanol, cyclohexane, chloroform, methanol, and copper nitrate ($Cu(NO_3)_2{\cdot}3H_2O$) were obtained from Beijing Chemical Reagent Company. *N*, *N*-dibutyldithiocarbamic acid (HS_2CNBut_2) was obtained from Beijing Ke'ao Technology co. Ltd. Prodium iodide (PI), liquid LB culture media, and solid LB culture media were supplied by Beijing Ke'ao Technology co. Ltd. The amphiphilic polymer PSI_{OAm} used for surface coating nanoparticles was prepared according to our previous protocol.[58-60] Except where stated otherwise, all the reagents were of analytical grade and used as received without further purification.

Characterization.

Transmission electron microscopy (TEM) images were obtained on a Hitachi H-800 transmission electron microscope with an acceleration voltage of 100 kV. High-resolution transmission electron microscopy (HRTEM) observations were performed on a JEOL JEM-2100F transmission electron microscope operating at 200 kV. Powder X-ray diffraction (XRD) patterns were recorded on a Bruker AXS D8-Advanced X-ray diffractometer with Cu Kα radiation (λ = 1.5418 Å). A 2θ ranging from 10° to 70° was carried out in steps of 0.02° with a count time of 2 s. UV-*vis*-NIR absorbance spectra of the as-synthesized Cu_7S_4 nanorods were measured with a UV-3600 spectrophotometer (Shimadzu) equipped with a plotter unit. The fluorescence imaging of bacteria was conducted on a TCS SP5 two-photon confocal microscopes (Leica) equipped with a Mai Tai near infrared (NIR) diode laser. The thermal imaging and temperature evolution plots were performed on a FLIR-A600 infrared (IR) camera. Cytotoxicity of these Cu_7S_4 nanocomposites was tested *via* an ELISA plate reader (F50, TECAN).

Synthesis of Cu_7S_4 Nanorods.

The $[Cu(S_2CNBut_2)_2]$ precursor was synthesized prior to the preparation of the hydrophobic Cu_7S_4 semiconductor nanorods. Typically, HS_2CNBut_2 (2.1 mg, 0.01 mL) and $Cu(NO_3)_2{\cdot}3H_2O$ (0.1 mmol) were mixed in ethanol (1.0 mL) under stirring and ultrasonication for 15 min. Subsequently, the ethanol was removed by evaporation and the product was dissolved in oleylamine (1.0 mL). The resultant green $[Cu(S_2CNBut_2)_2]$ solution was stored at room temperature for later use.

Next, a reaction flask equipped with a magnetic stirring bar was charged with 4.0 mL of OAm and 6.0 mL of ODE. The mixture was then gradually heated to 205 °C with a gentle flow of nitrogen with stirring. Then 1.0 mL of the as-prepared $Cu(S_2CNBut_2)_2$ precursor (0.1 mmol) was directly injected into the above hot solution, and the resultant solution turned into black instantly. This solution was maintained at 190 °C for 10 min and then cooled to 60 °C naturally by removing the heating metal block. A black product was obtained by addition of ethanol (30 mL) to the reaction mixture and subsequent centrifugation. The final product (Cu_7S_4 NRs) was collected by washing twice with hexane and precipitating with ethanol, and then re-dispersed in 1.0 mL of chloroform for later use. It

should be mentioned that we previously prepared small Cu_7S_4 nanoplates using a similar protocol with dodecanethiol (DDT) and excess HS_2CNBut_2.[56] In this work, Cu_7S_4 nanorods were obtained by changing the dosage of the ligands (See Table S1). The reason for the failure to obtain nanorods during the previous work may be ascribed to the strong chelating ability of dodecanethiol and HS_2CNBut_2 towards the Cu_7S_4 surface, which limits the epitaxial growth of the Cu_7S_4 nanocrystals. To be specific, in our previous work, excess HS_2CNBut_2 and DDT ligands were attached on the surface of Cu_7S_4 nanocrystals, which would stabilize or limit the epitaxial growth of them. However, when fewer ligands were employed in this work, the surface energy may drive the crystal growth at certain facet, leading to formation of nanorods.

Surface Functionalization of Hydrophobic Cu_7S_4 Nanorods.

The hydrophobic Cu_7S_4 nanorods (0.5mL, 300 μg) were transferred into the water phase by coating with a thin layer of the as-prepared amphiphilic PSI_{OAm} before photothermal ablation. In a typical procedure, 60 mg of the lab-made PSI_{OAm} and 300 μg of hydrophobic Cu_7S_4 nanorods were dissolved in chloroform (1 mL). The mixture was then added to 10 mL of NaOH aqueous solution (10 mmol L^{-1}) under ultrasonication, and a resultant brown emulsion was obtained. This emulsion was then kept at 60 °C for 2 h with stirring to remove chloroform. The Cu_7S_4 NCs were collected by centrifugation, and re-dispersed in deionized water (1.0 mL) for later application.

Evaluation of Photothermal Performance.

To measure the photothermal conversion efficiency of the hydrophilic Cu_7S_4 NCs, simulated sunlight was applied to irradiate the nanomaterial colloidal solution (1.0 mL) in a quartz cuvette under different power densities and concentrations of NCs. The irradiation power was set in the range of 0–1.0 W/cm^2, and the power density was measured through an optical power meter. The temperature profiles versus power or Cu_7S_4 NCs dosage were recorded by an online-type thermocouple thermometer with an accuracy of ±0.1 °C. To evaluate the solar photothermal efficiency of the NCs, the temperature variation of the aqueous dispersion was recorded versus time under continuous irradiation by simulated sunlight with a power density of 1.0 W/cm^2 until the solution reached a steady temperature.

Cell Viability Assay.

Cytotoxicity of the as-prepared nanocomposites was evaluated using a standard MTT assay. Briefly, HeLa cells (~5×10^4 cells/well) were seeded in a 96-well microtiter plate, then different amounts of Cu_7S_4 NCs (0 to 300 μg/mL) were added and exposed to irradiation by the simulated sunlight prior to incubation at 37 °C for 24 h under 5% CO_2 and a 95% relative humidity atmosphere, respectively. Then, 10 μL of sterile-filtered MTT stock solution in phosphate buffer solution (4.0 mg/mL) was added to each well. The 96-well microtiter plate was incubated at 37 °C for another 3 h. The absorbance of the soluble coloured formazan produced by cellular reduction of MTT in each well was measured at 490 nm using an ELISA plate reader (F50, TECAN), which corresponds to the cell viability.

Bacterium Culture.

Before each microbiological experiment, all samples and glassware were sterilized by autoclaving at 121 °C for 20 min. 10 μL of cryopreserved *S. aureus* or *E. coli* was transferred to 10 mL of liquid LB culture medium, respectively, and grown at 37 °C for 20 h whilst been shaken. Subsequently, the bacteria were centrifuged and re-dissolved in 10 mL of phosphate buffer solution (PBS, pH 7.4), which is called original bacterium solution. Prior to use, the original bacterium solution was then diluted to a concentration of 10^6 colony forming units per mL (CFU/mL) with PBS.

Viable Counting of Bacteria.

In order to observe the number of the bacterium colonies, the original bacterium solution (50 μL) was placed on LB solid medium by the spread plate method and cultured for 24 h, and then the number of bacteria was counted.

Photothermal Anti-bacterial Evaluation.

The bacterium suspension (200 μL, 10^7 CFU mL^{-1}) was mixed with Cu_7S_4 NCs (500 μL, 300 μg/mL) and PBS to afford a solution with total volume of 2.0 mL. The resulting solution was exposed to irradiation by simulated sunlight at a power density of 1.0 W/cm^2. Different irradiation times were investigated. After irradiation, 50 μL of the bacterium solution was spread on the solid LB culture medium pre-loaded in the agar plate, and then cultured for 24 h to evaluate the photothermal anti-bacteria efficiency. Both in the absence and presence of irradiation by simulated sunlight, the control experiments were conducted under identical conditions except that the NCs were replaced by the same volume of PBS. Then irradiation by natural sunlight at power density of 70 mW/cm^2 was used to evaluate the photothermal anti-bacterial efficiency.

Fluorescence Imaging Assay of Bacteria After Photothermal Treatment.

The bacteria after photothermal treatment were stained with PI (10 μg/mL) for 20 min in dark for fluorescence imaging. The dead bacterial cells were visualized (under a 100× lens) with a CLSM confocal microscope (Leica) equipped with a He-Ne laser (543 nm).

Results and discussion

Synthesis and Characterization of Cu_7S_4 NRs.

The Cu_7S_4 nanorods were synthesized by the hot-injection of freshly prepared $Cu(S_2CNBut_2)_2$ precursors in the presence of a mixed solvent consisting of OAm and ODE. As shown by the transmission electron microscope (TEM) images, these hydrophobic Cu_7S_4 nanocrystals demonstrated rod like shape with size of 50 nm × 13 nm, and no aggregation was observed (Figure 1a). After encapsulating with a thin layer of

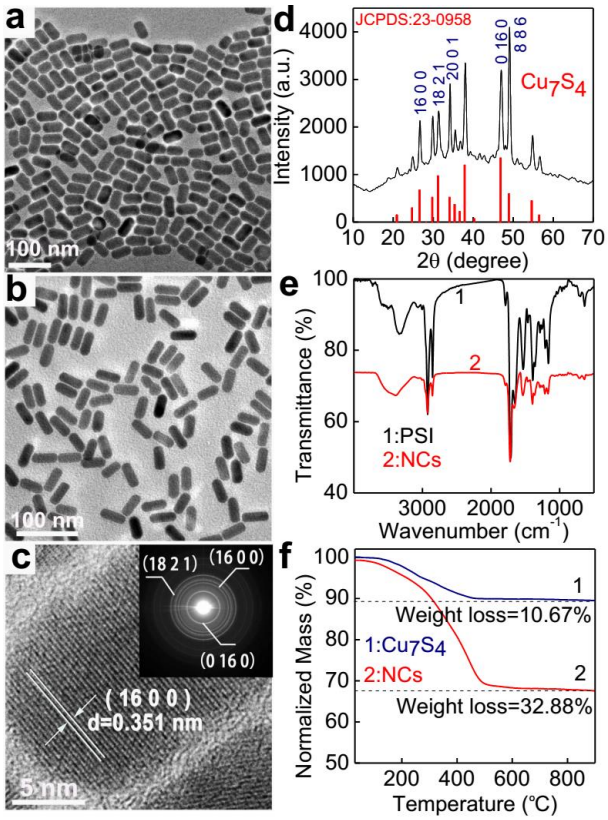

Fig. 1. TEM images of hydrophobic Cu_7S_4 NRs (a) and hydrophilic Cu_7S_4 NCs (b), HRTEM image of Cu_7S_4 NRs (c). Inset was the ED pattern of Cu_7S_4 NRs. d) XRD pattern of Cu_7S_4 NRs. e) FTIR spectra of PSI_{OAm} and Cu_7S_4 NCs. f) TGA profiles of the hydrophobic Cu_7S_4 NRs and hydrophilic Cu_7S_4 NCs.

PSI_{OAm} using a modfified version of our previously published procedure,[58] these hydrophobic NRs were successfully transferred from chloroform into water as Cu_7S_4 NCs and displayed superior water dispersibility (Figure 1b). Both of the hydrophobic and hydrophilic nanocrystals showed good size and shape distribution, and the dimensions of hydrophilic NRs remained unchanged before and after the phase transfer process. Furthermore, microstructure was determined by high-resolution transmission electron microscope (HRTEM) image (Figure 1c) and electron diffraction (ED) pattern (inset of Figure 1c). An interplanar spacing of 0.351 nm was observed in a single crystal from the HRTEM image, which corresponds to the *d*-spacing for (16 0 0) planes of the monoclinic Cu_7S_4 crystal. Additionally, the diffraction rings of the selected area ED pattern (Figure 1c) can be assigned to the (0 16 0), (16 0 0) and (18 2 1) zone axis of monoclinic Cu_7S_4 NRs, respectively. The monoclinic structures of these Cu_7S_4 NRs were further identified using powder X-ray diffraction (XRD) results (JCPDS card no. 23-0958) (Figure 1d). The coating layer surrounded the nanorod was further confirmed using Fourier transform infrared spectroscopy (FTIR) (Figure 1e) and thermogravimetric analysis (TGA) (Figure 1f). As shown in Figure 1e, the FTIR spectrum of Cu_7S_4 NCs is very similar to that of PSI_{OAm}, suggesting the successful coating of Cu_7S_4 with PSI_{OAm}. Moreover, from the TGA (Figure 1f), about 33% weight loss was observed from the Cu_7S_4 NCs, which was over

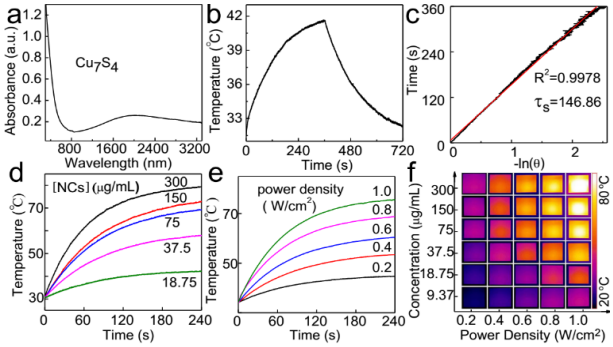

Fig. 2. a) UV-*vis* NIR spectrum of Cu_7S_4 NRs (solid state). b) The monitored temperature profiles of Cu_7S_4 NCs irradiated by laser for 360 s, followed by naturally cooling with laser light turned off. An 808-nm laser with power density of 0.457 W/cm^2 was used. c) Time constant (τ_s) for heat transfer from the system was determined to be 146.86 s by applying the linear time data from the cooling period of (b) *versus* negative natural logarithm of driving force temperature. d) Temperature increment over a period of exposure to the simulated sunlight (1.0 W/cm^2) at various NCs concentrations. e) Temperature increment *versus* irradiation power density over a period of exposure to the simulated sunlight. The concentration of NCs was 300 μg/mL. f) The photothermal image array of Cu_7S_4 NCs photothermal performance *versus* different power densities and concentrations. The irradiation time was 6 min.

three times than that (<11%) of hydrophobic Cu_7S_4 NRs, further indicating the successful encapsulation of Cu_7S_4 with PSI_{OAm}.

Photothermal Performance.

Prior to evaluation of the photothermal anti-bacteria activity, the photothermal performance of these Cu_7S_4 NCs was investigated. As shown in Figure 2a, these Cu_7S_4 NCs possess strong and broadband (300-3300 nm) absorption with a LSPR peak (1790 nm) in the near infrared (NIR) range, which is beneficial for efficient photothermal conversion of sunlight. The photothermal conversion efficiency of these Cu_7S_4 NCs was further investigated. To be specific, the Cu_7S_4 NCs dispersion was continuously illuminated by an 808-nm diode laser with a power density of 0.457 W/cm^2 for 360 s. Thereafter, the laser irradiation was switched off while the temperature was monitored to determine the rate of heat transfer within the system (Figure 2b, 2c). According to Roper's method[61] and our previous report,[56] the photothermal conversion efficiency (η_T) of these Cu_7S_4 NCs was calculated to be 57.8%. Herein, the stronger photothermal conversion efficiency achieved can be attributed to the larger size of the Cu_7S_4 nanorods compared to the small Cu_7S_4 nanoplates, because a large particle size favours photothermal conversion efficiency.[56, 62] It is worth noting that here we use a 808-nm laser considering that it is convenient for comparison with the previous work.[56] Of course, if the laser wavelength is close to the LSPR peak, higher photothermal conversion efficiency will be obtained. But in the current work, we are more concerned about the photothermal performance of these Cu_7S_4 NCs with irradiation of simulated and natural sunlight.

Therefore, we investigated the effects of NCs concentration and power density by simulated sunlight on the temperature evolution of the colloidal solution. As shown in Figure 2d, the

temperature profiles of Cu_7S_4 NCs at different concentrations (18.75-300 μg/mL) were measured under continuous irradiation using simulated sunlight with power density of 1.0 W/cm^2. The concentration of Cu_7S_4 NCs was calculated from Cu^{2+} concentration determined using inductively coupled plasma mass spectrometry (ICP-MS). The temperature elevated gradually along with an increase in the concentration of Cu_7S_4 NCs and reached 80 °C at the end. As expected, the power density of irradiation also has considerable influence on the temperature evolution (Figure 2e). When the power density is 1.0 W/cm^2, the temperature can rise to 80 °C from room temperature (25 °C) at NCs concentrations of 300 μg/mL, and even under a low power density of 0.4 W/cm^2, the temperature can reach 53 °C. In order to clearly and visually illustrate the photothermal performance with different power densities and concentrations of Cu_7S_4 NCs, the final photothermal images of the Cu_7S_4 NCs solution after irradiated by simulated sunlight for 6 min were also shown in Figure 2f, which implied that higher power density as well as concentrated Cu_7S_4 NCs gave the highest temperature increase. All the results suggest that our Cu_7S_4 NCs demonstrate excellent photothermal performance under irradiation by simulated sunlight, which is highly desirable for the sunlight induced photothermal anti-bacterial activity.

Anti-bacterial Tests.

Since photothermal agents for clinic and food sterilization require good biocompatibility and low cytotoxicity. We evaluated the cytotoxicity of the as-synthesized Cu_7S_4 NCs in HeLa cell lines, with and without irradiation by simulated sunlight (Figure S1, ESI†). In the absence of sunlight, the cell viability remains above 95% after incubation with Cu_7S_4 NCs (150 μg/mL) for 24 h. Further increasing the concentration of NCs up to 300 μg/mL, over 85% of cells were still alive. However, under irradiation by simulated sunlight (1.0 W/cm^2) for 5 min, the survival ratio of cells rapidly decreased, and finally the cell viability fell to less than 5% as a result of photothermal effect of Cu_7S_4 NCs. All these results suggest that the as-prepared Cu_7S_4 NCs are promising candidates for biocompatible and safe solar photothermal agents.

Encouraged by these excellent properties, we carried out the photothermal anti-bacteria performance of these Cu_7S_4 NCs. Two typical bacterial strains, i.e. Gram-positive *S. aureus* and Gram-negative *E. coli* whose shapes and sizes are shown in TEM images (Figure S2, ESI†), were selected as model bacteria to investigate. The bacterium number (colony) was counted using a serial dilution method (Figure S3, ESI†). The photothermal anti-bacteria efficiency of Cu_7S_4 NCs was assessed by the plate-count method with and without irradiation by simulated sunlight (Figure 3). As shown in Figure 3a, 3b, 3e and 3f, without sunlight irradiation, the survival ratio of bacteria was satisfied both for control (Figure 3a and 3e) and with NCs (Figure 3b and 3f), suggesting that the NCs alone cause negligible damage to the bacterial strains. However, after being exposed to irradiation by simulated sunlight (1.0 W/cm^2) for 3 min, the amount of bacteria remained almost unchanged

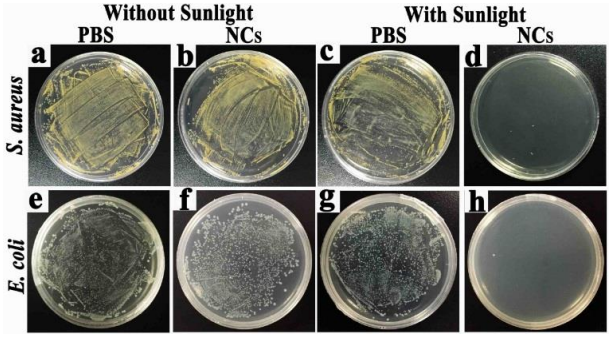

Fig. 3. Evaluation of photothermal antibacterial effects of Cu_7S_4 NCs on *S. aureus* (a-d) and *E.coli* (e-h) without (a, b, e and f) and with (c, d, g and h) the simulated sunlight (1.0 W/cm^2) irradiation for 3 min. The Cu_7S_4 NCs (500 μL, 300 μg/mL) and bacteria (200 μL, 10^7 CFU/mL) were mixed into PBS to afford a total volume of 2 mL solution and then irradiated with the simulated sunlight (1.0 W/cm^2) for 3 min. After irradiation, 50 μL of the bacterium suspension was cultured in the agar plate and incubated at 37 °C for 24 h before photographing and counting. As controls, the phosphate buffer solution (PBS) instead of Cu_7S_4 NCs colloidal solution was mixed with the bacteria before sunlight exposure in group a, c, e and g.

in the absence of photothermal agents (Figure 3c and 3g), while the bacteria were completely killed in the presence of Cu_7S_4 NCs (75 μg/mL) (Figure 3d and 3h), demonstrating the outstanding broad spectrum disinfectant efficiency of Cu_7S_4 NCs. The influence of the irradiation time (0, 0.5, 1, 2, 3, 4 min) on the photothermal anti-bacterial efficiency was also investigated by taking *E.coli* (Figure S4, ESI†) and *S. aureus* (Figure S5, ESI†) as model bacteria. The results indicated that under a power density of 1.0 W/cm^2, an exposure time of 2 and 3 min was sufficient for the complete eradication of *E. coli* and *S. aureus*, respectively. To explore the possible disinfection mechanism of the as-prepared Cu_7S_4 NCs, we have carried out the control experiments by treating bacteria suspension with heat since it is generally recognized that the extensive LSPR features of Cu_7S_4 NCs can give rise to photothermal effect. In order to evaluate the influence of such effect on the disinfection, we heated up the sample for 4 min under temperature of 70 °C in the dark environment. As shown in Figure S6 (ESI†), clearly, it was found that if only treated with heat, both *E. coli* and *S. aureus* colonies were still observed in the agar plate, indicating the incompleteness of disinfection of this method. While, for the sample treated under simulated sunlight (Figure 3d, 3h), the bacteria were completed killed as no bacteria colony was found in the agar plate. Therefore, these results indicated that the antibacterial property of Cu_7S_4 NCs was not just originated from the photothermal effect. We propose both photothermal effect and solar light driven catalytic activity account for the observed high antibacterial efficiency.

In addition, a red fluorescence dye (prodium iodide, PI) was utilized for further evaluating the photothermal anti-bacterial efficiency given that the membrane of bacterial was destroyed after photothermal treatment and the PI can stain the dead bacterial. As shown in Figure 4, lots of *S.aureus* and *E.coli* cells either live or dead were observed from the bright-field microscopy images (Figure 4, a1-d1 and e1-h1). As expected, the bright red fluorescence of PI was only observed from *S. aureus* (Figure 4d) and *E. coli* (Figure 4h) bacteria treated with photothermal agents under the simulated sunlight irradiation,

indicating that these bacteria were dead under the photothermal effect of these agents. In addition, it is clear that in the absence of either photothermal agents (Figure 4a, c, e, g) or sunlight (Figure 4a, b, e, f), the growth of bacteria was not influenced. These results further suggest that our Cu_7S_4 NCs are efficient photothermal agents for disinfection using irradiation by a source of simulated sunlight.

To illustrate the potential applications in the wild and environmental treatment, we further evaluated the photothermal anti-bacteria efficiency of these Cu_7S_4 NCs with natural sunlight as irradiation source. As shown in Figure 5, in the presence of Cu_7S_4 NCs (75 μg/mL), even though the power density of natural sunlight was as low as 70 mW/cm^2, both bacterial strains were totally killed after being exposed to natural sunlight for 10 min (Figure 5b and 5d). As controls, no obvious antibacterial effect was observed in the absence of Cu_7S_4 NCs under the same irradiation conditions (Figure 5a and 5c). These results suggest that the as-prepared Cu_7S_4 NCs can effectively absorb natural sunlight irradiation and convert the solar energy to heat, implying that these highly doped copper chalcogenide semiconductor nanocrystals can serve as promising solar photothermal agents with wide applications, such as antibacterial therapy, food sterilization, and environmental treatment, especially for applications in the wild and at disaster scenes where special laser equipment is not available.

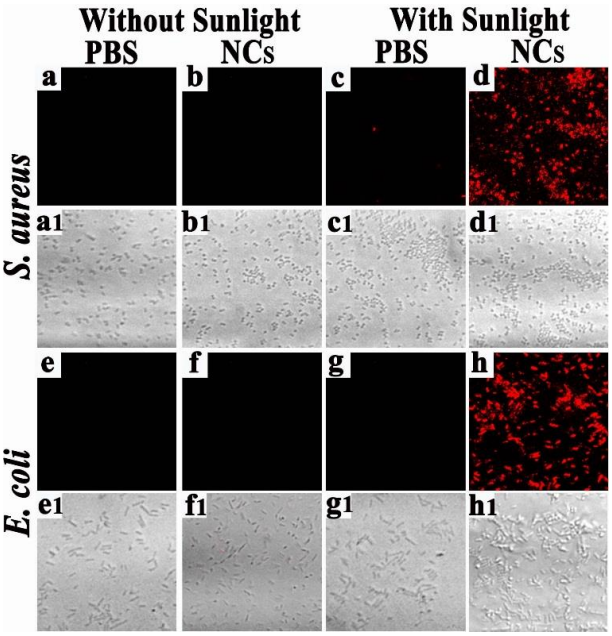

Fig. 4. Fluorescence (a-d and e-h) and bright-field (a1-d1 and e1-h1) imaging of *S. aureus* (a-d and a1-d1) and *E. coli* (e-f and e1-f1) under different treatments. (a, b, a1, b1, e, f, e1, f1) without and (c, d, c1, d1, g, h, g1, h1) with the simulated sunlight irradiation (1.0 W/cm^2) for 3 min. (a, c, a1, c1, e, g, e1, g1) without photothermal agent and (b, d, b1, d1, f, h, f1, h1) with 75 μg/mL of Cu_7S_4 NCs dispersed in PBS solution. To observe the fluorescence images of dead bacteria, both of the *S. aureus* and *E.coli* were stained with 10 μg/mL of PI for 20 min (red indicates dead bacterial). The excitation wavelength was set at 543 nm.

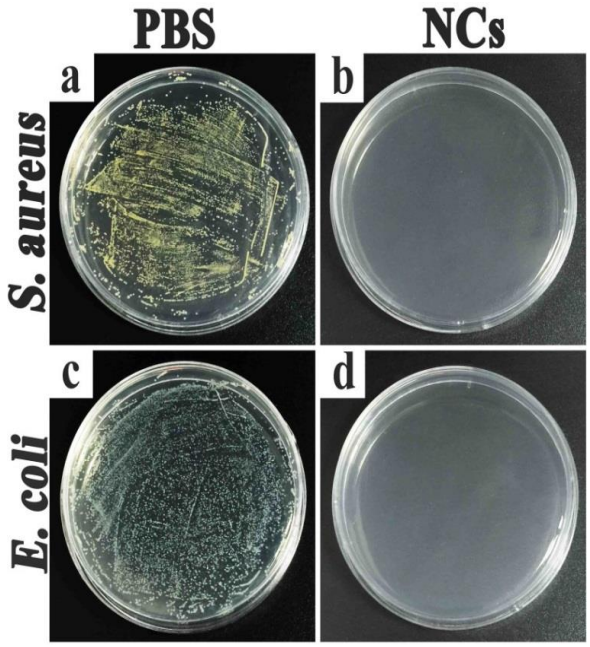

Fig. 5. Evaluation of photothermal anti-bacteria efficiency of Cu_7S_4 NCs on *S. aureus* (a, b) and *E.coli* (c, d) with natural sunlight (70 mW/cm^2) irradiation for 10 min. The Cu_7S_4 NCs (500 μL, 300 μg/mL) and bacteria (200 μL, 10^7 CFU/mL) were mixed into PBS to afford a total volume of 2 mL solution and then irradiated with the natural sunlight (70 mW/cm^2) for 10 min. After irradiation, 50 μL of the bacterium suspension was cultured in the agar plate and incubated at 37 °C for 24 h before photographing and counting.

Conclusion

In conclusion, we developed a green and efficient, photothermal fungicide agent, Cu_7S_4 NRs, which enable to directly use sunlight for highly efficient disinfection. The monodisperse Cu_7S_4 NRs was prepared *via* a new strategy by using hot injection and thermolysis of a single precursor and the resultant hydrophobic Cu_7S_4 NRs were then successfully transferred into aqueous solution by surface coating using an amphiphilic polymer PSI_{OAm}. The as-prepared Cu_7S_4 NCs display broadband absorption and excellent photothermal conversion efficiency, thus afford greatly enhanced antibacterial efficiency towards both Gram-positive (*S. aureus*) and Gram-negative (*E. coli*) bacteria. Under natural sunlight irradiation (70 mW/cm^2), in the presence of a rather low concentration of the photothermal agents, both of the bacteria strains were completely killed after being exposed for 10 min. In addition to high photothermal conversion efficiency and broadband absorption, these Cu_7S_4 nanocrystals also possess other favourable features such as earth-abundance, low toxicity, good biocompatibility and high stability, which would be ideal for further use in an economic and eco-friendly manner. This proof-of-concept experiment paves the way to explore inexpensive and highly efficient photothermal agents with broadband absorption for directly employing clean and renewable solar energy for various applications in clinics and food sterilization and environmental treatment.

Acknowledgements

This research was supported in part by the National Natural Science Foundation of China (Grant Nos. 21475007, 21275015 and 21505003), and the Fundamental Research Funds for the Central Universities (YS1406, buctrc201507 and buctrc201608). We also thank the support from the "Innovation and Promotion Project of Beijing University of Chemical Technology", the "Public Hatching Platform for Recruited Talents of Beijing University of Chemical Technology, the High-Level Faculty Program of Beijing University of Chemical Technology (buctrc201325), and BUCT Fund for Disciplines Construction and Development (Project No. XK1526)".

Notes and references

1. S. G. Wang, A. K. Singh, D. Senapati, A. Neely, H. T. Yu and P. C. Ray, *Chem.-Eur. J.*, 2010, **16**, 5600-5606.
2. Y. Zhu, M. Ramasamy and D. K. Yi, *ACS Appl. Mater. Interfaces*, 2014, **6**, 15078-15085.
3. K. H. Choi, H. J. Lee, B. J. Park, K. K. Wang, E. P. Shin, J. C. Park, Y. K. Kim, M. K. Oh and Y. R. Kim, *Chem. Commun.*, 2012, **48**, 4591-4593.
4. Y. Zhao, Y. Tian, Y. Cui, W. Liu, W. Ma and X. Jiang, *J. Am. Chem. Soc.*, 2010, **132**, 12349-12356.
5. X. N. Hu, Y. Y. Zhao, Z. J. Hu, A. Saran, S. Hou, T. Wen, W. Q. Liu, Y. L. Ji, X. Y. Jiang and X. C. Wu, *Nano Res.*, 2013, **6**, 822-835.
6. H. M. N. Iqbal, G. Kyazze, I. C. Locke, T. Tron and T. Keshavarz, *Green Chem.*, 2015, **17**, 3858-3869.
7. K. C. L. Black, T. S. Sileika, J. Yi, R. Zhang, J. G. Rivera and P. B. Messersmith, *Small*, 2014, **10**, 169-178.
8. B. Hu, N. Wang, L. Han, M. L. Chen and J. H. Wang, *Acta Biomater.*, 2015, **11**, 511-519.
9. J. Tang, Q. Chen, L. G. Xu, S. Zhang, L. Z. Feng, L. Cheng, H. Xu, Z. Liu and R. Peng, *ACS Appl. Mater. Interfaces*, 2013, **5**, 3867-3874.
10. Y. Y. Zhao, Z. Chen, Y. F. Chen, J. Xu, J. H. Li and X. Y. Jiang, *J. Am. Chem. Soc.*, 2013, **135**, 12940-12943.
11. E. G. Ju, Z. H. Li, M. Li, K. Dong, J. S. Ren and X. G. Qu, *Chem. Commun.*, 2013, **49**, 9048-9050.
12. B. H. Lai and D. H. Chen, *Acta Biomater.*, 2013, **9**, 7573-7579.
13. Z. Fan, D. Senapati, S. A. Khan, A. K. Singh, A. Hamme, B. Yust, D. Sardar and P. C. Ray, *Chem.-Eur. J.*, 2013, **19**, 2839-2847.
14. T. F. Tian, X. Z. Shi, L. Cheng, Y. C. Luo, Z. L. Dong, H. Gong, L. G. Xu, Z. T. Zhong, R. Peng and Z. Liu, *ACS Appl. Mater. Interfaces*, 2014, **6**, 8542-8548.
15. Y. W. Wang, Y. Y. Fu, L. J. Wu, J. Li, H. H. Yang and G. N. Chen, *J. Mat. Chem. B*, 2013, **1**, 2496-2501.
16. Y. Wang, J. Wan, R. J. Miron, Y. Zhao and Y. Zhang, *Nanoscale*, 2016, **8**, 11143-11152.
17. B. Liu, C. Li, Z. Cheng, Z. Hou, S. Huang and J. Lin, *Biomaterials science*, 2016, **4**, 890-909.
18. J. Liu, X. P. Zheng, L. Yan, L. J. Zhou, G. Tian, W. Y. Yin, L. M. Wang, Y. Liu, Z. B. Hu, Z. J. Gu, C. Y. Chen and Y. L. Zhao, *ACS Nano*, 2015, **9**, 696-707.
19. W. W. Li, P. F. Rong, K. Yang, P. Huang, K. Sun and X. Y. Chen, *Biomaterials*, 2015, **45**, 18-26.
20. K. C. Li, H. C. Chu, Y. Lin, H. Y. Tuan and Y. C. Hu, *ACS Appl. Mater. Interfaces*, 2016, **8**, 12082-12090.
21. Z. Q. Meng, F. Wei, R. H. Wang, M. G. Xia, Z. G. Chen, H. P. Wang and M. F. Zhu, *Adv. Mater.*, 2016, **28**, 245-253.
22. Q. W. Tian, M. H. Tang, Y. G. Sun, R. J. Zou, Z. G. Chen, M. F. Zhu, S. P. Yang, J. L. Wang, J. H. Wang and J. Q. Hu, *Adv. Mater.*, 2011, **23**, 3542-3547.
23. R. Z. Zhong, C. Peng, L. Chen, N. Yu, Z. X. Liu, M. F. Zhu, C. L. He and Z. G. Chen, *RSC Adv.*, 2016, **6**, 40480-40488.
24. S. H. Kim, E. B. Kang, C. J. Jeong, S. M. Sharker, I. In and S. Y. Park, *ACS Appl. Mater. Interfaces*, 2015, **7**, 15600-15606.
25. C. W. Hsiao, H. L. Chen, Z. X. Liao, R. Sureshbabu, H. C. Hsiao, S. J. Lin, Y. Chang and H. W. Sung, *Adv. Func. Mater.*, 2015, **25**, 721-728.
26. Y. N. Xia, W. Y. Li, C. M. Cobley, J. Y. Chen, X. H. Xia, Q. Zhang, M. X. Yang, E. C. Cho and P. K. Brown, *Acc. Chem. Res.*, 2011, **44**, 914-924.
27. Y. C. Wang, K. C. L. Black, H. Luehmann, W. Y. Li, Y. Zhang, X. Cai, D. H. Wan, S. Y. Liu, M. Li, P. Kim, Z. Y. Li, L. H. V. Wang, Y. J. Liu and Y. N. Xia, *ACS Nano*, 2013, **7**, 2068-2077.
28. F. Hu, Y. Zhang, G. C. Chen, C. Y. Li and Q. B. Wang, *Small*, 2015, **11**, 985-993.
29. M. Ramasamy, S. S. Lee, D. K. Yi and K. Kim, *J. Mat. Chem. B*, 2014, **2**, 981-988.
30. X. M. Dai, Z. Fan, Y. F. Lu and P. C. Ray, *ACS Appl. Mater. Interfaces*, 2013, **5**, 11348-11354.
31. Q. Zhang, J. Ge, J. Goebl, Y. Hu, Y. Sun and Y. Yin, *Adv. Mater.*, 2010, **22**, 1905-1909.
32. P. C. Ray, S. A. Khan, A. K. Singh, D. Senapati and Z. Fan, *Chem. Soc. Rev.*, 2012, **41**, 3193-3209.
33. D. H. Lin, T. Q. Qin, Y. Q. Wang, X. Y. Sun and L. X. Chen, *ACS Appl. Mater. Interfaces*, 2014, **6**, 1320-1329.
34. B. Z. Ristic, M. M. Milenkovic, I. R. Dakic, B. M. Todorovic-Markovic, M. S. Milosavljevic, M. D. Budimir, V. G. Paunovic, M. D. Dramicanin, Z. M. Markovic and V. S. Trajkovic, *Biomaterials*, 2014, **35**, 4428-4435.
35. X. J. Yang, Z. H. Li, E. G. Ju, J. S. Ren and X. G. Qu, *Chem.-Eur. J.*, 2014, **20**, 394-398.
36. M. C. Wu, A. R. Deokar, J. H. Liao, P. Y. Shih and Y. C. Ling, *ACS Nano*, 2013, **7**, 1281-1290.
37. W. Y. Pan, C. C. Huang, T. T. Lin, H. Y. Hu, W. C. Lin, M. J. Li and H. W. Sung, *Nanomedicine : nanotechnology, biology, and medicine*, 2016, **12**, 431-438.
38. B. Li, Q. Wang, R. J. Zou, X. J. Liu, K. B. Xu, W. Y. Li and J. Q. Hu, *Nanoscale*, 2014, **6**, 3274-3282.
39. C. V. Durgadas, K. Sreenivasan and C. P. Sharma, *Biomaterials*, 2012, **33**, 6420-6429.
40. S. S. Chou, B. Kaehr, J. Kim, B. M. Foley, M. De, P. E. Hopkins, J. Huang, C. J. Brinker and V. P. Dravid, *Angew. Chem. Int. Ed.*, 2013, **52**, 4160-4164.
41. L. Cheng, J. J. Liu, X. Gu, H. Gong, X. Z. Shi, T. Liu, C. Wang, X. Y. Wang, G. Liu, H. Y. Xing, W. B. Bu, B. Q. Sun and Z. Liu, *Adv. Mater.*, 2014, **26**, 1886-1893.
42. J. T. Hou, Y. Z. Li, M. Y. Mao, Y. Z. Yue, G. N. Greaves and X. J. Zhao, *Nanoscale*, 2015, **7**, 2633-2640.
43. F. Liu, M. Zeng, Y. Z. Li, Y. Yang, M. Y. Mao and X. J. Zhao, *Adv. Func. Mater.*, 2016, **26**, 4518-4526.
44. Y. Ma, Y. Z. Li, M. Y. Mao, J. T. Hou, M. Zeng and X. J. Zhao, *J. Mater. Chem. A*, 2015, **3**, 5509-5516.
45. M. Y. Mao, Y. Z. Li, J. T. Hou, M. Zeng and X. J. Zhao, *Appl. Catal. B*, 2015, **174**, 496-503.
46. Y. L. Zheng, W. Z. Wang, D. Jiang, L. Zhang, X. M. Li and Z. Wang, *J. Mater. Chem. A*, 2016, **4**, 105-112.
47. X. Q. Huang, S. H. Tang, X. L. Mu, Y. Dai, G. X. Chen, Z. Y. Zhou, F. X. Ruan, Z. L. Yang and N. F. Zheng, *Nat. Nanotechnol.*, 2011, **6**, 28-32.

48. C. B. Gao, J. Goebl and Y. D. Yin, *J. Mater. Chem. C*, 2013, **1**, 3898-3909.
49. Y. D. Yin and D. Talapin, *Chem. Soc. Rev.*, 2013, **42**, 2484-2487.
50. L. Zhang, T. Z. Liu, K. Liu, H. Lu, Y. D. Yin and C. B. Gao, *Nano Lett.*, 2015, **15**, 4448-4454.
51. Q. Zhang, J. P. Ge, T. Pham, J. Goebl, Y. X. Hu, Z. D. Lu and Y. D. Yin, *Angew. Chem. Int. Ed.*, 2009, **48**, 3516-3519.
52. S. Pramanik, S. Chattopadhyay, J. K. Das, U. Manju and G. De, *J. Mater. Chem. C*, 2016, **4**, 3571-3580.
53. L. Zhang and Z. S. Wang, *J. Mater. Chem. C*, 2016, **4**, 3614-3620.
54. Z. H. Wu, Q. Zeng and H. S. Wang, *J. Mater. Chem. C*, 2016, **4**, 2614-2620.
55. S. Cho, M. J. Lee, M. S. Kim, S. Lee, Y. K. Kim, D. H. Lee, C. W. Lee, K. H. Cho and J. H. Chung, *J. Dermatol. Sci.*, 2008, **50**, 123-133.
56. J. B. Cui, R. Jiang, S. Y. Xu, G. F. Hu and L. Y. Wang, *Small*, 2015, **11**, 4183-4190.
57. J. M. Luther, P. K. Jain, T. Ewers and A. P. Alivisatos, *Nat. Mater.*, 2011, **10**, 361-366.
58. S. Huang, M. Bai and L. Y. Wang, *Sci Rep.*, 2013, **3**, 2023-2028.
59. S. Huang, S. Peng, Y. B. Li, J. B. Cui, H. L. Chen and L. Y. Wang, *Nano Res.*, 2015, **8**, 1932-1943.
60. N. N. Tu and L. Y. Wang, *Chem. Commun.*, 2013, **49**, 6319-6321.
61. D. K. Roper, W. Ahn and M. Hoepfner, *J. Phys. Chem. C*, 2007, **111**, 3636-3641.
62. M. Zhou, R. Zhang, M. A. Huang, W. Lu, S. L. Song, M. P. Melancon, M. Tian, D. Liang and C. Li, *J. Am. Chem. Soc.*, 2010, **132**, 15351-15358.

